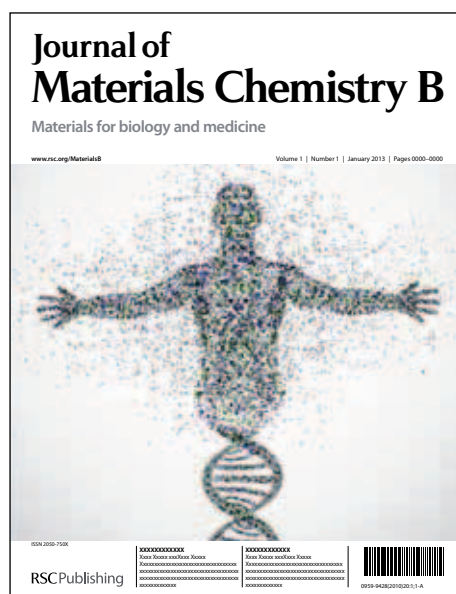


Journal of Materials Chemistry B

Accepted Manuscript



This is an *Accepted Manuscript*, which has been through the RSC Publishing peer review process and has been accepted for publication.

Accepted Manuscripts are published online shortly after acceptance, which is prior to technical editing, formatting and proof reading. This free service from RSC Publishing allows authors to make their results available to the community, in citable form, before publication of the edited article. This *Accepted Manuscript* will be replaced by the edited and formatted *Advance Article* as soon as this is available.

To cite this manuscript please use its permanent Digital Object Identifier (DOI®), which is identical for all formats of publication.

More information about *Accepted Manuscripts* can be found in the [Information for Authors](#).

Please note that technical editing may introduce minor changes to the text and/or graphics contained in the manuscript submitted by the author(s) which may alter content, and that the standard [Terms & Conditions](#) and the [ethical guidelines](#) that apply to the journal are still applicable. In no event shall the RSC be held responsible for any errors or omissions in these *Accepted Manuscript* manuscripts or any consequences arising from the use of any information contained in them.

Cite this: DOI: 10.1039/c0xx00000x

Paper

www.rsc.org/materials

Intrinsically Radiolabeled Multifunctional Cerium Oxide Nanoparticles for *in vivo* Studies

Likun Yang,^a Gobalakrishnan Sundaresan,^a Minghao Sun,^a Purnima Jose,^a David Hoffman,^a Philip Reed McDonagh,^a Narottam Lamichhane,^a Cathy S Cutler,^b J. Manuel Perez^c and Jamal Zweit^{*a}

Received (in XXX, XXX) Xth XXXXXXXXX 200X, Accepted Xth XXXXXXXXX 200X

DOI: 10.1039/b000000x

Cerium oxide nanoparticles (CONP) have demonstrated protection properties against oxidation damages in various cells and tissues. The mechanism of this, however, is poorly understood. Monitoring the interaction of CONP with biological compartments 'in situ' is crucial to understand their biochemical and physiological properties *in vivo*. In this paper, a multifunctional nanoparticle platform was obtained through intrinsic radiolabeling strategy and extrinsic surface functionality to combine dual imaging components (Single Photon Emission Computed Tomography/Optical Imaging, SPECT/OI) in one nanoparticle. The cell viability, cell uptake and overall *in vivo* biodistribution of CONP were also manipulated through surface functionalization. The intrinsic radiolabeling strategy is demonstrated by incorporating radionuclides (¹⁴¹Ce, ¹¹¹In or ⁶⁵Zn) into CONP and radiolabeled CONP (rCONP) was coated with biocompatible polymers including Dextran T10 (DT10), Poly(acrylic acid) (PAA), or functionalized DT10 (DT10-NH₂, DT10-PEG and DT10-sulfobetaine). Fluorescent CONP was obtained through conjugation of fluorescein isothiocyanate (FITC) with DT10-NH₂ rCONP and used for cell imaging. The DT10 and DT10-NH₂ rCONP did not show decreased viability up to 120 µg/mL whilst the PAA rCONP showed decreased viability beyond 40 µg/mL. Variations in blood circulation and renal/hepatic clearance of rCONP were demonstrated and were dependent on surface coating and hydrodynamic size of nanoparticles. The *ex vivo* biodistribution results were reflected in SPECT imaging of ¹⁴¹Ce-rCONP, showing accumulation in liver and spleen in a living mouse over a one week period. The intrinsic radiolabeling and extrinsic surface modifications together determine the biophysical properties of CONP and their potential applications for *in vivo* studies and biomedical imaging.

1. Introduction

Nanomedicine is poised to provide a "step change" in the advancement of medical care through the application of nanoscience and nanotechnology. Several inorganic/organic based nanoparticles (NPs), including quantum dots, paramagnetic NPs, noble metal NPs, silicon oxide NPs, liposome and polymer NPs are emerging as promising nanomaterials. They have unique potential in biomedicine, as diagnostic and/or therapeutic agents (theranostic), due to their specific physiochemical properties and structural characteristics. In oncology, nanomedicine platforms could enable targeted delivery of imaging agents and therapeutics to cancerous tissue and serve as drug delivery vehicles with the potential of site-specific drug release.¹⁻⁴

Cerium oxide nanoparticles (CONP) have unique properties in free radical scavenging.⁵⁻⁹ The CONP is a rare-earth metal oxide NP of the lanthanide series, which is widely used in ultraviolet absorbance,¹⁰ oxygen sensing^{11, 12} and automotive catalytic converters.^{13, 14} This NP has both Ce³⁺ and Ce⁴⁺ oxidation states that could result in an auto-regenerative redox cycle between Ce³⁺

and Ce⁴⁺, accompanied by creation of oxygen defects on their surface and offers many active sites for free radical scavenging.⁵⁻⁹ A potential application of CONP to quench reactive oxygen species (ROS) in biological systems is currently being investigated. For example, studies have demonstrated that CONP are able to confer neuronal,¹⁵ ocular,¹⁵ radio-protection,¹⁶⁻¹⁹ in addition to protection of heart from oxidative and inflammatory injury induced by cardiac-specific expression of monocyte chemoattractant protein-1.²⁰ Furthermore, it has been reported that CONP can mimic the properties of superoxide dismutase (SOD), an endogenous cellular defense against free radicals.²¹ Thus, CONP may represent a novel agent to protect cells and tissues from damage by its regenerative free radical scavenging properties. However, the *in vivo* mechanisms underlying this unique property are poorly understood, due to the lack of *in vivo* detection and imaging tools for these NPs. Since CONP does not have inherent detection capability, quantitative and tomographic imaging of these unique NPs has not been possible. In addition, the radiotracer technique and *in vivo* imaging will uniquely contribute, not just to the understanding of *in vivo*

pharmacokinetics, but will also serve as a quantitative tool to better understand *in vivo* toxicology, an important aspect for all nanoparticle-based agents. Although, some fluorescent dyes, such as ampliflu,²² have been used to label CONP for fluorescent imaging, this approach has inherent limitations, including poor tissue penetration, scattered fluorescent signal and lack of true quantitation, and more importantly, no potential for clinical translation.

Surface modification of NPs plays a key role in determining their *in vitro* and *in vivo* physicochemical and biochemical properties.^{23,24} The intrinsic radiolabeling method, described here, provides a robust strategy to monitor the *in vivo* behaviour of NPs without interfering with the external surface properties. Enhanced *in vivo* stability of intrinsically radiolabeled NPs will also enable studies for long-term imaging, tissue interactions and toxicology mechanisms.²⁵⁻²⁸

In this work, we have developed a method to synthesize multifunctional intrinsically radiolabeled CONP (rCONP) incorporating gamma-emitting radionuclides, thereby providing a quantitative *in vivo* tool to study and image the behaviour of various CONPs. We also modified external surface properties of rCONPs with various biocompatible macromolecules, including Poly(acrylic acid) (PAA), Dextran T10 (DT10) and functionalized DT10 to vary hydrodynamic size, surface charge and functional groups of CONPs. Through this surface engineering, manipulation of *in vitro* cell viability and *in vivo* pharmacokinetics of rCONPs can be achieved and monitored by radiotracer analysis and real time SPECT imaging. The surface modification of rCONP with Fluorescein isothiocyanate (FITC) produces fluorescent nanoprobe which can be used for cell fluorescent imaging. This strategy also paves the way for further targeted imaging and therapeutic application of rCONPs. For example, we are currently investigating the use of CONP in normal tissue protection from free radical damage, during radiation therapy, in which the rCONP described here, will provide an *in vivo* tool to study such phenomenon.

2. Experimental

2.1 Chemicals and characterization

All chemicals were used as received without further purification. Cerium(III) Nitrate hexahydrate (99.0%), ammonium hydroxide solution (30%), poly(acrylic acid) (PAA, $M_w=1,800$), hydrogen peroxide (H_2O_2), N,N'-disuccinimidyl carbonate (DSC), ethylenediamine, N,N-diisopropylethylamine (DIPEA), polyethylene glycol 600 (PEG 600), N,N-dimethylethylenediamine (98%) and fluorescein isothiocyanate (FITC) (99%) were obtained from Sigma-Aldrich (USA). Dextran T10 (DT10, $M_w=10,000$) was purchased from pharmacosmos (Denmark). Di-tert-butyl dicarbonate (97%) was purchased from Alfa Aesar (USA). Cerium-141 chloride ($^{141}CeCl_3$, half life: 32.53 days, specific activity: 9.54 mCi/mg) was supplied from University of Missouri Research Reactor. Indium-111 chloride ($^{111}InCl_3$, half life: 2.83 days, specific activity: 415.8 mCi/mg) and zinc-65 chloride ($^{65}ZnCl_2$, half life: 244 days, specific activity: 4.28 mCi/mg) were purchased from Perkin Elmer (USA).

Zeta Sizer Nano Series ZEN3600 (Malvern, USA) was used to

measure the hydrodynamic size and zeta potential of rCONPs in water. UV-vis absorption and fluorescent emission spectra of FITC labeled rCONP were recorded using Beckman Coulter DU730 and Varian Cary eclipse spectrophotometer respectively. 1H NMR spectra were recorded at 300 MHz on a Varian Mercury 300 spectrometer with solvent proton resonance as reference. ICP measurements were carried out on a Vista-MPX CCD Simultaneous ICP-OES (Varian, USA). Gamma counter (LKB Wallac 1282 compugamma CS universal gamma counter/Perkin Elmer, USA) was calibrated for ^{141}Ce using an energy window centered on 145 keV. Thermal gravimetric analysis (TGA) measurement was operated on TGA Q5000 (TA Instruments, USA.) under nitrogen flow, heating rate is $10^\circ C/min$.

2.2 Production of Cerium-141

Cerium-141 was produced at the University of Missouri Research Reactor through an (n, γ) reaction, $^{140}Ce + ^1_0n \rightarrow ^{141}Ce$.

Briefly, 1-3 mg of natural CeO_2 was irradiated at a flux of 2×10^{14} n/cm²/s for approximately 155 hr. The target was processed 24 hr post irradiation to allow for short lived impurities to decay. The irradiated cerium oxide was dissolved in 2 mL of a 1:1 mixture of 30% H_2O_2 and 6 M nitric acid heated at $90^\circ C$ until all the powder was completely dissolved. Heat was then used to take the target to dryness. HCl (2 mL, 0.05 M) was added once the solution was close to dryness. The process was repeated three times to ensure all nitric acid was removed. The final dissolution was performed with 500 μL of 0.05 M HCl. A small volume was taken for high purity germanium counting to assess the radionuclidic purity, which was greater than 98% four days after end of irradiation.

2.3 Synthesis of 2-amino-ethyl sulfobetaine (2-amino-ethyl-SB)

To a solution of N,N-dimethylethylenediamine (1.24 mL, 11.3 mmol), in dried dichloromethane (20 mL), was added dropwise the solution of di-tert-butyl carbonate (2.6 g, 11.9 mmol) in dichloromethane (5 mL) slowly at $4^\circ C$ under rigorous stirring. The reaction was kept overnight at room temperature (r.t). The reaction mixture was washed with brine three times. Combined organic phase was dried by anhydrous Na_2SO_4 . Removal of solvent gives the product tert-butyl 2-(dimethylamino)ethylcarbamate as colorless oil (2.0 g, 93%).

1H NMR (300 MHz, $CDCl_3$): δ 5.02 (s, 1H), 3.20 (t, 2H), 2.36 (t, 2H), 2.20 (s, 6H), 1.43 (s, 9H).

The solution of tert-butyl 2-(dimethylamino)ethylcarbamate (2.0 g, 10.6 mmole) and 1,3-propane sultone (1.66 g, 13.6 mmole) in anhydrous chloroform (20 mL) was heated to $60^\circ C$ under stirring overnight. The precipitate was collected and washed three times with chloroform (3 x 10 mL) to produce BOC-protected 2-amino-ethyl-SB as a white solid (3.27 g, 99%).

1H NMR (300 MHz, D_2O): δ 7.42 (s, 1H), 3.71-3.65 (m, 2H), 3.60-3.57 (m, 4H), 3.30 (s, 6H), 2.76-2.70 (m, 2H), 2.26-2.20 (m, 2H), 1.65 (s, 9H).

Deprotection of BOC-protected 2-amino-ethyl-SB (3.2 g, 10.3 mmole) was performed in a HCl aqueous solution (pH= 0~1) to give 2-amino-ethyl-SB as a colorless oil (2.86 g, 96%).

1H NMR (300 MHz, D_2O): δ 3.75-3.70 (m, 2H), 3.61-3.52 (m, 4H), 3.22 (s, 6H), 2.99 (t, 2H), 2.28-2.23 (m, 2H).

Amino methoxy poly(ethylene glycol) (Amino-PEG-600) was synthesized according to literature.²⁹

2.4 Synthesis of functionalized Dextran T10

Dextran T10 (DT10) (1.0 g, 0.1 mmol, Mw: 10 K Da) (contains 18.5 mmol hydroxyl groups) was dissolved in DMSO (10 mL) with gentle heating then cooled to r.t. DIPEA (0.64 mL, 3.67 mmol) and DSC (0.48 g/0.96 g/1.44 g, 1.87 mmol/ 3.74 mmol/ 5.61 mmol) in DMSO/DMF (2/2 mL) was added dropwise to the resultant solution with stirring to activate the hydroxyl groups.³⁰

The reaction mixture was left for 3 hrs at r.t and corresponding amount of amino derivatives (2-amino-ethyl-SB or amino-PEG-600 or N,N-dimethylethylenediamine) dissolved in DMSO or DMF or H₂O (1.5 mL, 1.87 mmol) was added to the reaction mixture swiftly. The reaction was kept overnight at r.t while stirring. Functionalized DT10 (DT10-SB, DT10-PEG or DT10-NH₂) was dialyzed against DI water (dialysis cassette, molecular weight cut off: 2,000 Da) then dried under vacuum. The pH of DT10-SB and DT10-PEG in H₂O is about 7.0 and DT10-NH₂ is about 9.0-10.0. The functional degree was tuned as 10%, 20% or 30%. DT10-SB-20%, DT10-PEG-20% and DT10-NH₂-10% were selected for further investigation.

DT10-SB: ¹H NMR (300 MHz, D₂O): δ 4.99 (m), 3.97-3.93 (m), 3.73 (m), 3.56 (m), 3.19 (s), 3.00 (t), 2.26 (m).

DT10-PEG: ¹H NMR (300 MHz, D₂O): δ 5.00 (m), 4.02-3.99 (m), 3.95-3.91 (m), 3.72 (m), 3.66-3.54 (m), 3.40 (s).

DT10-NH₂: ¹H NMR (300 MHz, D₂O): δ 4.95 (m), 3.95-3.91 (m), 3.70 (m), 3.57-3.50 (m), 3.20-3.15 (m), 2.70 (s), 2.20 (s), 1.41-1.31 (m).

2.5 Synthesis of PAA or DT10 coated rCONPs (PAA rCONP or DT10 rCONP)

Ce(NO₃)₃·6H₂O (1 mg, 0.0025 mmol) and polymers (PAA or DT10) (25 mg) were dissolved in 1.5 mL DI water. The water solution of ¹⁴¹CeCl₃ (or ⁶⁵ZnCl₂ or ¹¹¹InCl₃) (400 μCi) was added and allowed to digest for 1 hr. The above solution was added dropwise to NH₄OH (3 mL, 0.7 M) slowly and the resulting reaction was kept 24 hrs at r.t while stirring. The reaction solution was centrifuged at 4,000 rpm for 30 min and filtered through a 0.22 μm nylon syringe filter. The filtered solution was then centrifuged to separate ammonium hydroxide and unreacted PAA or DT10, and concentrated with Amicon filters (30,000 MWCO) at 10,000 rpm for 30 min. The cut-off solution was collected and diluted by DI water. The reaction yields calculated from ICP and gamma counting are listed in Table 1.

2.6 Synthesis of DT10-PEG-20% or DT10-SB-20% rCONPs (DT10-PEG rCONP or DT10-SB rCONPs)

According to the same synthetic procedure of DT10 rCONP, the reaction yield is 80%-85% for DT10-PEG and DT10-SB rCONP determined by ICP. Radiolabeled reaction yield with ⁶⁵Zn is 45%-49% determined from gamma counting.

2.7 Synthesis of DT10-NH₂-10% rCONP (DT10-NH₂ rCONP)

Following the same synthetic procedure of DT10 rCONP, pH of DT10-NH₂ (25 mg) solution in water (1.5 mL) was adjusted to 7.0 with 4 M aqueous HCl prior to reaction.

2.8 Bioconjugation of DT10-NH₂ rCONP with FITC (FITC-DT10 rCONP) and determination of ratio of dye/rCONP

DT10-NH₂ rCONP (13.6 nmole) was dissolved in sodium bicarbonate solution (0.1 M, 100 μL, PH: 8.3~8.5) and then

added dropwise with FITC solution (264.5 μg, 680 nmole, 260 μL). Reaction was incubated for 4 hrs at r.t. The reaction mixture was purified with Amicon filters (30,000 MWCO) at 10,000 rpm for 30 min. Unreacted FITC was removed by washing with DI water (3 x 0.5 mL). Ratio of dye/rCONP in FITC-DT10 rCONP was determined by measuring UV-vis absorption of dye (at maximum Abs peak) and concentration of Ce. Briefly, a standard curve of dye in water was prepared and used to calibrate the Abs intensity of dye conjugated rCONP to determine the molar concentration of organic dye. The concentration of rCONP was determined by ICP.

2.9 ICP measurement

DT10, PAA, DT10-NH₂, DT10-SB, DT10-PEG or FITC-DT10 rCONP solution was diluted with 7% nitric acid solution (trace metal content nitric acid in nanopure water) and left to digest for 3 days. The concentration of Ce (ppm) was calculated based on the calibrated standard curve. Atomic absorption peak of Ce at 446 nm was selected to measure the absorption of rCONP solution.

2.10 Gel Filtration Chromatography (GFC)

DT10 ¹⁴¹Ce-rCONP, DT10-PEG and DT10-SB coated ⁶⁵Zn-rCONP were analyzed by RP-HPLC (Waters 1525, USA) on a 8 x 300 mm, 250 Å Diol (TOSOH, Japan) gel filtration column (TSKgel G3000 SWxl). Buffer containing 0.05 M Na₂HPO₄, 0.05 M NaH₂PO₄ and 0.15 M NaCl was used as mobile phase. Flow rate of the mobile phase was 1 mL/min. 25 μL (20 μCi) of the sample solution was injected onto the HPLC. The retention time of rCONP was monitored by a UV detector (254 nm, model 2489, Waters, USA) and a radio-detector (B-FC-3300, Bio-Scan, USA).

2.11 Autocatalytic activity of radiolabeled and surface functionalized CONPs

Concentration of Ce in each functionalized DT10 rCONP solution was determined by ICP. The final concentration was standardized to 1.15 mg/mL. 3 mL of each solution was used to monitor the autocatalytic activity by the percentage transmittance. 10 μL of 1 M H₂O₂ was added to each sample to oxidize CONP. The percentage transmittance was then monitored upon addition of H₂O₂ immediately and at 1, 4/5, 7 and 10 days. The solution of CONP without H₂O₂ was used as control.

2.12 Cell cultures

Cell lines of human epidermoid carcinoma (KB 3-1), colorectal adenocarcinoma (COLO 205), lung carcinoma (A549) and ovarian adenocarcinoma (SK-OV-3) were maintained under standard culture conditions (37° C and 5% CO₂) in a humid environment. Briefly, KB 3-1 cells were grown in DMEM/High glucose medium supplemented with 10% fetal bovine serum (FBS), 5 mM L-Glutamine and 1X Penicillin/Streptomycin (Pen-Strep). COLO 205 cells were cultured in RPMI-1640 medium supplemented with 10% heat inactivated FBS and 1X Pen-Strep. A549 cells were grown in F-12 medium supplemented with 10% heat inactivated FBS and 1X Pen-Strep, while SK-OV-3 cells were grown in McCoy's 5A medium supplemented with 10% heat inactivated FBS and 1X Pen-Strep. The cells were grown to 70-80% confluency before using in the experiments. KB 3-1 cells

were obtained from Dr. M Gottesman (NCI, Bethesda, MD), COLO 205 from ATCC (USA), A549 and SK-OV-3 were purchased from NCI Tumor/Cell line Repository (Frederick, MD).

2.13 Cell viability assay

Cell Titer-Glo Luminescent Cell Viability Assay kit (Promega, USA) was used to evaluate the cell viability of CONP on KB 3-1, COLO 205, A549 and SK-OV-3 cells. Briefly, 10^4 cells were plated in opaque 384-well plates in triplicates for each concentration (0.5, 1, 5, 10, 40, 80 and 120 $\mu\text{g}/\text{mL}$) and treated with increasing concentrations of DT10, DT10-NH₂ and PAA rCONP for 24 hrs. At the end of incubation period Cell Titer-Glo reagent was added to untreated and each treatment groups. The cell viability was assessed by measuring the luminescence, detected by a multimode detector (Beckman Coulter, USA). The luminescent signal generated is directly proportional to the ATP produced by metabolically active cells. The luminescence detected in untreated cells was used as control (100% viability) to calculate percent viability in treatment groups. Statistical analysis was performed using Student's t-test. P value of <0.05 was considered statistically significant. Microsoft Excel software was used for all statistical analysis.

2.14 Cell uptake study using rCONPs

To study the uptake of DT10, DT10-NH₂ and PAA rCONP by COLO 205 and KB 3-1 cells, $0.6\text{--}0.8 \times 10^6$ cells were seeded in 6-well plates in 10% complete growth medium and allowed to adhere overnight. After overnight culture, the medium was replaced with 1% serum containing complete growth medium. The cells were then treated with 1 $\mu\text{g}/\text{mL}$ DT10 or DT10-NH₂ rCONP for periods of 15 min, 30min, 1 hr, 2 hrs and 4 hrs or 1 $\mu\text{g}/\text{mL}$ PAA rCONP for 1 hr and 4 hrs. At the end of incubation period the supernatant was collected and an aliquot was used for gamma counting. The cells in the plate were thoroughly and gently rinsed with PBS and the wash buffer collected and spun down to collect any non-adherent/loosely adherent cells in the wash and finally mixed with the adherent cells. The adherent cells in the plate were lysed using radioimmunoprecipitation assay buffer (RIPA buffer, Pierce, USA). An aliquot of the cell lysate was used for gamma counting and for measuring the amount of protein in each well.

2.15 Fluorescent labeling of cells with FITC-DT10 rCONP

COLO 205 and KB 3-1 cells were incubated with FITC-DT10 rCONP at 1 $\mu\text{g}/\text{mL}$, 5 $\mu\text{g}/\text{mL}$ or 12.5 $\mu\text{g}/\text{mL}$ concentrations for 4 hrs. Cells were then washed three times with PBS and fixed with 4% paraformaldehyde. FITC-DT10 rCONP labeled cells were then imaged under inverted fluorescence microscope, Olympus IX-71 with built-in Nuance Multispectra Image System (Perkin Elmer, USA).

2.16 Biodistribution

Animal experiments were performed according to the policies and guidelines of the Institutional Animal Care and Use Committee (IACUC) at Virginia Commonwealth University. Adult female nude mice (Harlan, USA) were injected with the solution of PAA or DT10 rCONP in saline (6-7 μCi , 200 μL , ~140 pmole) via the tail vein. The body weight of animals used in

this study averaged 20.2 ± 2.1 grams (mean \pm sd). Mice were euthanized and blood samples and major organs were collected at various time points after injection (5 min, 1 hr, 4 hrs, 24 hrs, 48 hrs, 120 hrs; $n=3$ per time point). The radioactivity of each sample was measured by gamma counting. The percent injected dose per gram (%ID/g) of tissues was calculated from gamma counting.

2.17 In vivo SPECT/CT imaging

Micro-SPECT was performed using an Inveon SPECT system (Siemens, USA) having dual-head camera mounted with 2 multipinhole collimators (five 1.0-mm pinholes in each collimator, 60-mm trasaxial FOV, 40-mm radius of rotation and maximum resolution of 1.5 mm). Images were acquired over 360° in a total of 40 projections, resulting in a total imaging time of 90 min. One nude mouse (20.3 grams body weight) was intravenously injected with DT10 ¹⁴¹Ce-rCONP (182 μCi , 335 μL , 3.6 nmole, specific activity is 50.6 mCi/ μmol) and 110 min later, was anesthetized with mixture of 2% isoflurane in oxygen and whole body micro-SPECT imaging was carried out as described above. A 6 min whole body Micro-CT scan was also performed using the Inveon micro-CT scanner (Siemens, USA) with 75 kV and 500 μA at a resolution of 96 μm . SPECT/CT images were acquired at 2, 24, 72 and 144 hrs post injection. The SPECT images were reconstructed using an iterative reconstruction algorithm (ordered-subset expectation maximization or OSEM3D) modified for the 5-pinhole geometry with a 20% energy window around the 145 keV photopeak of ¹⁴¹Ce. These images were automatically registered with CT images based on a transformation matrix previously generated using four ⁵⁷Co landmarks. Images were viewed and quantified using ASIpro VM, an image data analysis software (Concord Microsystems, USA). Organ regions of interest (ROIs) were drawn and the %ID/g values were calculated.

3. Results and discussion

3.1 Radiosynthesis and characterization of rCONPs

Synthetic methods of cerium oxide nanoparticles, including sol-gel, thermal decomposition, solvo-thermal oxidant, micro-emulsion, flame spray pyrolysis and co-precipitation have been investigated previously.³¹ Among them, co-precipitation is commonly used "in situ" strategy to achieve uniform water soluble and biocompatible CONP under mild reaction conditions. In our study, three isotopes (¹⁴¹Ce, ¹¹¹In and ⁶⁵Zn) were used to dope CONP by co-precipitation synthesis (Fig. 1A).³²⁻³⁶ ¹⁴¹Ce radiolabeling yield was greater than 97% for DT10 rCONP (Table 1); similar yield was obtained for ¹¹¹In. The yield of ⁶⁵Zn radiolabeling ranged from 80% to 88% for DT10 rCONP. Radiolabeling of CONP was confirmed by GFC. The retention times of ¹⁴¹Ce-rCONP and ⁶⁵Zn-rCONP were 6-8 min, which correspond to the retention time of CONP whilst the retention time for ⁶⁵ZnCl₂ was 15 min. The results of GFC-HPLC provide evidence for the successful incorporation of the radionuclide into CONP (Radio-HPLC chromatograms are shown in Fig. S1 for DT10 ¹⁴¹Ce-rCONP, DT10-PEG and DT10-SB coated ⁶⁵Zn-rCONP as well as ⁶⁵ZnCl₂).

The reaction yield of rCONP was dependant on the surface coating ligands used in the reaction. Table 1 shows the reaction

yield of different surface coated rCONP determined by ICP and gamma counting. Quantitative radiosynthesis yields were achieved for DT10 and DT10-NH₂ rCONP and determined by both ICP (stable Ce) and gamma counting (¹⁴¹Ce). However, obvious lower reaction yields of PAA rCONP were observed, which could be due to the lower reactivity of PAA with the Ce ion. Selection of ligands will not only influence surface properties, size and biological properties of rCONP but also affect the radioactive reaction yield.

Table 1 Hydrodynamic size, surface charge and reaction yield of different surface functionalized ¹⁴¹Ce-rCONP

	Average size (nm)	Zeta potential (mV) ^a	Reaction yield by ICP (%)	Reaction yield by gamma counting (%)
DT10 rCONP	6.0	-5.0	97.4±1.6	97.0±0.3
PAA rCONP	2.0	-40.6	69.4±6.8	74.7±9.6
DT10-NH ₂ rCONP	9.0	34.2	~100	99.5±0.2

^aMeasured at pH 7.4 aqueous solution.

Hydrodynamic size (HD size) and the surface charge of rCONP were characterized by dynamic light scattering (DLS) and zeta potential measurement (Table 1). It is interesting to note that the size of CONP synthesized by co-precipitation is strongly dependent on the synthetic procedure and surface coating

polymer. For instance, HD size of DT10 rCONP showed a uniform size distribution of about 6.0 nm in water (Fig. S2A). As a comparison, the HD size of PAA rCONP is smaller, and showed two size distributions at 2.0 nm (about 93%) and 5.3 nm (about 7%) (Fig. S2B). HD size of DT10-NH₂ rCONP can be tuned to 2.0 nm or 9.0 nm (Fig. S2C and F), depending on the reaction procedure. The adjusted size and distribution of CONPs synthesized by different reaction schemes and surface coating ligands indicate that polymers used for coating CONPs profoundly impact the nucleation and growth of NPs. The tunable size and surface functionalization of CONP make it feasible to improve their physiological properties and influence pharmacokinetics *in vivo*.

3.2 Surface modification of rCONPs

Surface modification of NPs affects their stability, biocompatibility, cytotoxicity, intracellular internalization and *in vivo* pharmacokinetics. In our study, glucose, cyclodextran, mannose, maltose, PAA, DT10 and PEG were applied to functionalize CONP. Carbohydrate monomer or oligomer or PEG coating resulted in lower reaction yields and poor stability of CONP. PAA rCONP showed smaller HD size, good stability and higher uptake but higher cytotoxicity and lower biocompatibility during *in vitro* and *in vivo* experiments. However, DT10 rCONP showed excellent aqueous stability and biocompatibility.

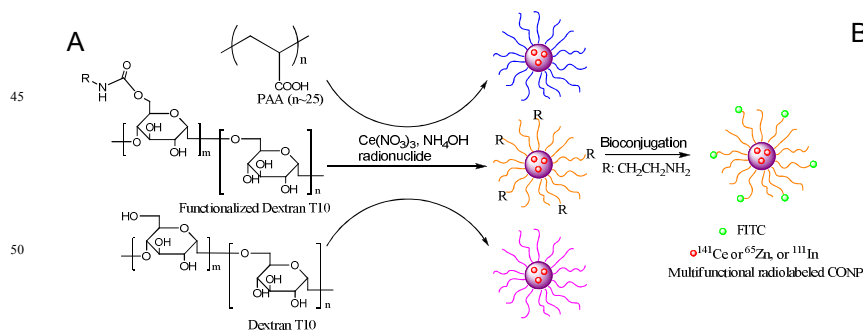


Fig. 1 (A) Synthetic scheme of multifunctional rCONP and (B) UV-vis absorption and fluorescence spectra (insert) of FITC, DT10-NH₂ rCONP and FITC-DT10 rCONP in H₂O.

DT10 rCONP could be stored over 6 months under ambient conditions without obvious aggregation from DLS measurement. However, the hydroxyl groups of DT10 are relatively inert to further functionalization of CONP. The reactive functional groups, such as amine, carboxylic acid or thiol are commonly used for bioconjugation of NPs with other biomolecules or organic dyes. In our work, a highly reactive reagent N,N'-disuccinimidyl carbonate (DSC) was used to activate hydroxyl groups of DT10. Compounds containing amine were reacted with DSC activated hydroxyl to functionalize DT10 through formation of urethane. By this method, DT10 can be functionalized with many compounds and functional groups, such as PEG, zwitterionic sulfobetaine (SB), PEG-NH₂, etc. Functionalized DT10 is capable of reacting with Ce ion in the presence of ammonium hydroxide to form CONP under mild reaction conditions. The results of NMR indicate that the degree of functionalization is tunable (Fig. S3).

In our study, several compounds were selected to functionalize

DT10. The functionalization degree of DT10 can be controlled by activating different amounts of OH in DT10. Short chain amino-PEG (Mw=600), zwitterionic amino-SB or ethylenediamine were reacted with DT10 and functionalized DT10 can be used to coat CONP successfully without dramatically changing their HD size.

Synthesis of multifunctional DT10 coated rCONP is shown in Fig 1A. The reaction yield of synthesis of functional DT10 rCONP is slightly lower (80%-85%) than the DT10 reaction, which could be due to the decreased amounts of OH (reactive groups) in modified DT10 upon introduction of the new functional groups. Reduced amounts of OH could result in the decreased reaction yield of CONP synthesis.³⁷ Different from post surface functionalization of NPs, HD size of surface functionalized CONP coated by modified DT10 did not change from DLS measurement (Fig. S2). This provides a method to tune the surface charge or PEG density of CONP without changing their size. It will be beneficial to investigate the effect of surface coating of NPs on the biological behavior while keeping other

factors consistent.

Amino functionalized DT10 (10% functional degree) coated CONP was also synthesized using the same reaction strategy. Thermalgravimetric analysis (TGA) was used to determine the weight ratio of polymer coating to inorganic core of DT10-NH₂ CONP (Fig. S4). The weight of samples was constant after temperature reached 400°C under N₂ and about 80–85% weight loss was observed due to the decomposition of the organic layer. Based on the result of TGA and functional degree of DT10, we estimate that average 23–33 amine functionalized DT10 were coated on one CONP and a large number of primary amines (400–600) were combined in one CONP. However, it should be pointed out that most of the amino groups were buried in the polymer layer and are therefore not available for bioconjugation. This was confirmed by verifying the conjugation reaction of DT10-NH₂ rCONP with FITC. In the conjugation reaction, excess FITC was used and the free FITC was removed by filtration through a molecular weight cut-off filter after the conjugation reaction. From the combined results of UV-vis and ICP, it was estimated that ~10 FITC were linked to one rCONP. UV-vis absorption and emission of FITC-DT10 rCONP was compared with neat dye in water (Fig. 1B). UV-vis spectrum of FITC-DT10 rCONP showed two characterized peaks at 297 nm and 491 nm, which are attributed to absorption of CONP and FITC respectively. It is interesting that the fluorescent intensity of FITC-DT10 rCONP increased (by 3.5 fold) compared with neat dye at the same absorption (Fig. 1B insert). The fluorescent enhancement of organic dyes incorporated to NPs (covalent or noncovalent binding) had been reported previously.^{38, 39} By using this method, it is also feasible to link targeting molecules to rCONP, which could increase the active uptake of rCONP in tumors.

3.3 Redox properties of functionalized CONP

The unique redox process which relates to reversible transformation of Ce³⁺ ↔ Ce⁴⁺ within CONP is key for its specific application in radical scavenging and anti-inflammation.^{5–9} Perez *et al* showed that the autocatalytic property of DT10 CONP can be recovered within 10 days after addition of H₂O₂.¹¹ We investigated the redox properties of functionalized DT10 rCONP to illuminate the effect of surface functionalization or incorporation of radionuclides on the autocatalytic properties of CONP. An immediate color change was observed when H₂O₂ was introduced to the solution of DT10 rCONP or functional DT10 CONP (concentration of Ce: 1.15 mg/mL), indicating the oxidation of Ce³⁺ to Ce⁴⁺ within CONP. Red-shift transmission spectra of samples after addition of H₂O₂ was detected to gradually shift back and the color of the oxide sample change back to its original color of slight yellow, which indicates the autocatalytic reduction of Ce⁴⁺ to Ce³⁺ within CONP (Fig. 2 and Fig. S5). It is worth noting that, the reduction process of rCONP is faster (7 days) than the nonradiolabeled CONP (10 days). This reflects the improved autocatalytic redox capability of rCONP compared to CONP.^{5, 11} This was observed for all rCONP types regardless of the radionuclide used. The reason for the accelerated redox process of rCONP is still not clear but it is possible that the electron emitted from the radioisotope decay takes part in the reduction process of Ce⁴⁺ to Ce³⁺ in the CONP. The radionuclides act as electron donors to accelerate the redox

process and improve the redox property of rCONP. It is advantageous when rCONP is used as the diagnostic or therapeutic probe because the improved redox capability of rCONP can accelerate the reduction of ROS and reduce the response time.

Redox properties of functionalized DT10 coated CONP including DT10-PEG and DT10-SB CONP were investigated and similar phenomenon as DT10 CONP was observed (Fig. 2C and 2D). After 10 days of addition of H₂O₂, the reduction property of functionalized CONP was recovered completely. This indicated no influence of surface functionalization on the physicochemical properties of CONP. It is easy to understand that the redox is an inherent property of the inorganic core of CONP and different surface coatings shouldn't influence the ratio of Ce³⁺/Ce⁴⁺ in CONP. Three redox cycles were investigated over 30 days for all samples and no loss of redox capability of CONP was observed.

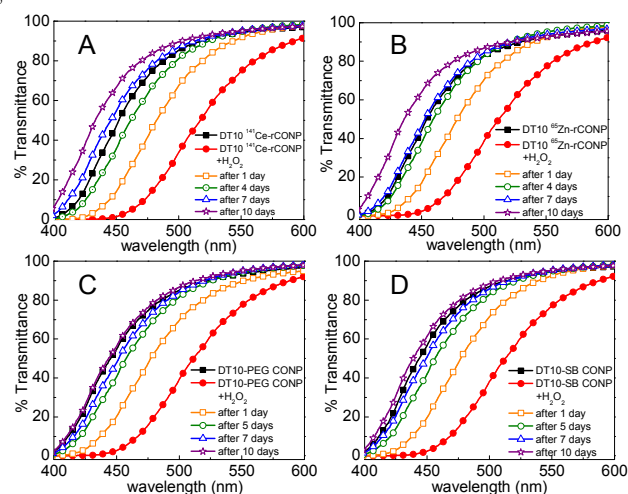


Fig. 2 Autocatalytic redox properties of (A) DT10 ¹⁴¹Ce-rCONP, (B) DT10 ⁶⁵Zn-rCONP, (C) DT10-PEG CONP and (D) DT10-SB CONP.

3.4 Cell viability, cell uptake and fluorescent labeling of multifunctional ¹⁴¹Ce-rCONP

In order to understand the relation of cytotoxicity of rCONP to their surface coating, cell viability of COLO 205, KB 3-1, A549 and SK-OV-3 cell lines, incubated with increasing concentrations of DT10, DT10-NH₂ and PAA ¹⁴¹Ce-rCONP was examined following 24 hrs incubation (Fig. 3A, 3B and Fig. S6). Incubation of cells with DT10 rCONP increased the cell viability of COLO 205 and KB 3-1 cells at 0.5 and 1.0 ug/ml concentrations. A similar increase in cell viability was also seen in A549 and SK-OV-3 cells when treated with up to 10 µg/ml concentrations of DT10 rCONP. DT10 rCONP did not show significant cytotoxicity up to 120 µg/mL for COLO 205, A549 and SK-OV-3. Cell viability of KB 3-1 dropped when treated with 120 µg/mL DT10 rCONP. It is usually believed that positively charged NPs show higher cytotoxicity⁴⁰ but the cells treated with DT10-NH₂ rCONP didn't have any significant cell toxicity at any of the concentrations tested except in KB 3-1, which indicates that the charge on the surface of NPs is not the only factor inducing cytotoxicity. However, all the cell lines exposed to high concentrations of PAA rCONP showed significant cell death. Exposure to concentrations of PAA rCONP at and above 40 µg/ml caused cell death in COLO 205 and KB 3-1 whereas

exposure from 10-120 $\mu\text{g/ml}$ concentration caused decreased cell viability in A549 and SK-OV-3 cells. These results indicate that cells are more tolerant of DT10 rCONP than PAA rCONP and exposure of the NH_2 group on the surface of rCONP does not

alter the sensitivity of the cells to rCONP. For *in vitro* uptake studies, relatively low concentrations of 1 $\mu\text{g/ml}$ DT10, DT10- NH_2 and PAA rCONP were selected to assess the accumulation of rCONP in COLO 205 and KB 3-1 cell lines with time. The results obtained from gamma counting are shown in Fig. 3C and 3D. All three coatings of rCONP showed gradually enhanced cell uptake with time. Further analysis on the number of NPs per cell was calculated based on the specific activity of rCONP and radioactivity per cell. At 1 hr, the uptake number of DT10, DT10- NH_2 and PAA rCONP by COLO 205 cells is 6.0×10^4 , 5.7×10^4 and 16.3×10^6 per cell respectively.

These values increased to 1.0×10^5 , 2.0×10^5 and 38.0×10^6 per cell after 4 hrs incubation. For KB 3-1 cells, the uptake number of DT10, DT10- NH_2 and PAA rCONP is 1.2×10^5 , 8.4×10^4 and 16.2×10^6 respectively. The number increased to 1.7×10^5 , 1.9×10^5 and 20.9×10^6 after 4 hrs incubation. Compared with DT10 and DT10- NH_2 rCONP, PAA rCONP showed higher cell uptake by both cell lines at 1 hr and 4hrs. This may be due to the smaller HD size of PAA rCONP. The cell uptake results can also be related to the cell viability results. The higher cytotoxicity of PAA rCONP could be due to its higher cell uptake, causing it to be more toxic than DT10 and DT10- NH_2 rCONP at the same concentration. These results show that radiolabeling provides a feasible method to quantitatively study the behavior of CONP *in vitro*.

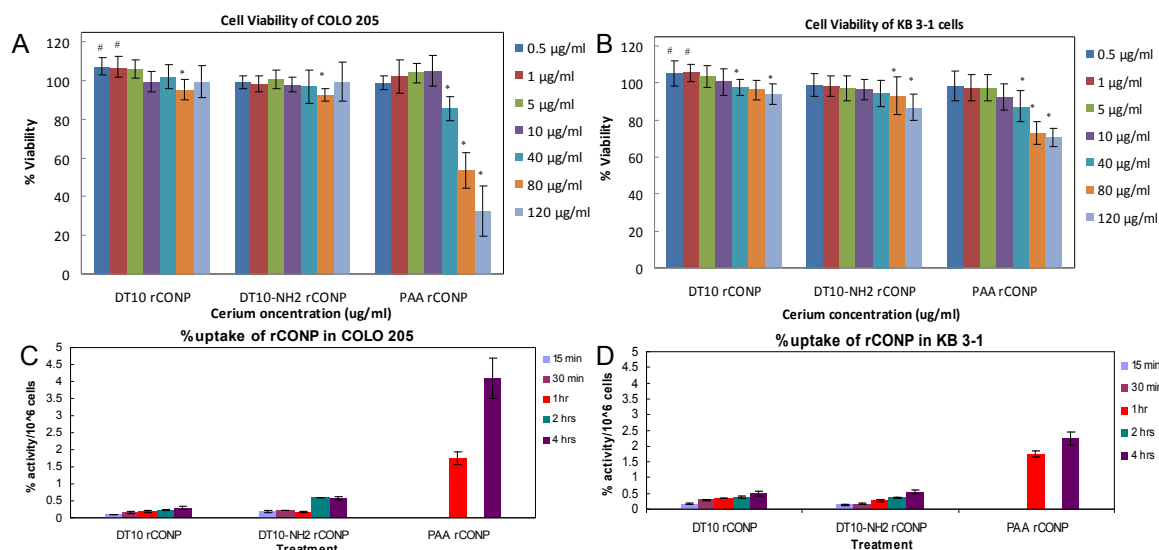


Fig. 3 Cell viability of (A) COLO 205 cells and (B) KB 3-1 cells after 24 hrs exposure to various cerium concentrations of DT10, DT10- NH_2 and PAA ^{141}Ce -rCONP. Data is expressed as mean % viability \pm SD. Significant increase or significant decrease in viability is indicated by # and *, respectively ($p < 0.05$). The cell uptake of 1 $\mu\text{g/ml}$ cerium concentration of DT10, DT10- NH_2 and PAA rCONP in (C) COLO 205 cells and (D) KB 3-1 cells at various time points was measured by gamma counting of ^{141}Ce radioactivity. For PAA ^{141}Ce -rCONP, cell uptake was measured at 1 hr and 4 hrs only.

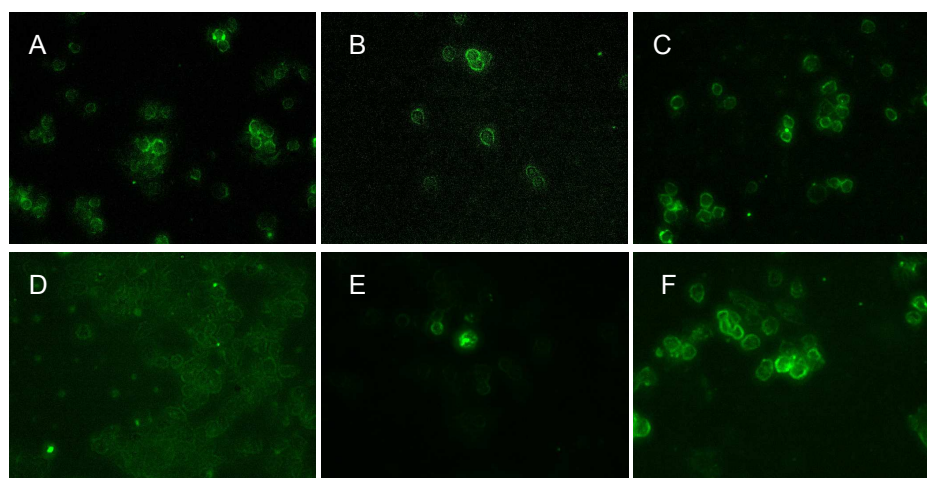


Fig. 4 Fluorescence microscopy images of FITC-DT10 rCONP labeled cells after 4 hrs incubation: (A) COLO 205, 1 $\mu\text{g/ml}$ of cerium; (B) COLO 205, 5 $\mu\text{g/ml}$; (C) COLO 205, 12.5 $\mu\text{g/ml}$; (D) KB 3-1, 1 $\mu\text{g/ml}$; (E) KB 3-1, 5 $\mu\text{g/ml}$ and (F) KB 3-1, 12.5 $\mu\text{g/ml}$.

To investigate the interaction of rCONP with the cells, fluorescent microscopy images of cells, after incubating with

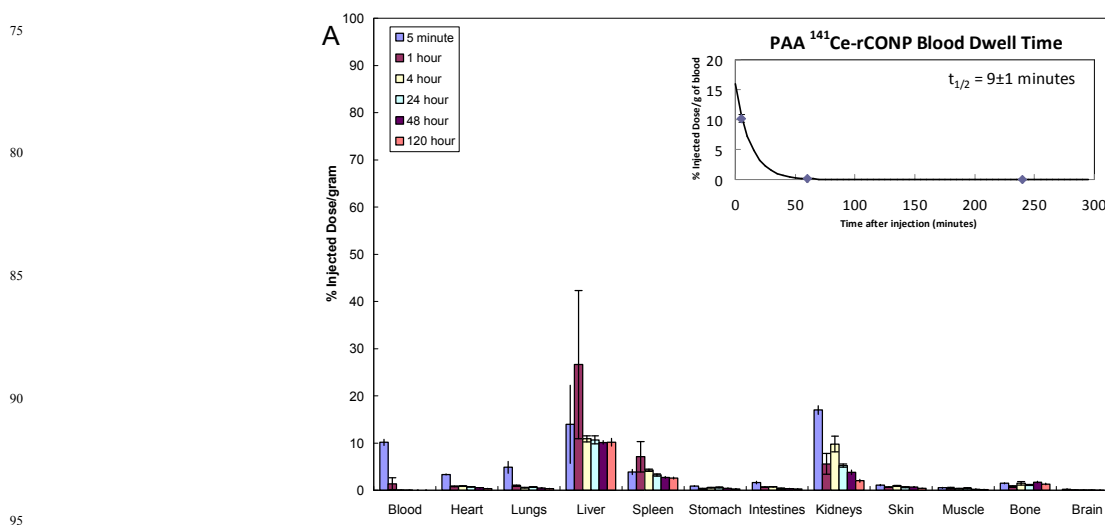
FITC-DT10 rCONP, were obtained. These images reveal that 4 hrs post incubation with 1 $\mu\text{g/ml}$ concentration of FITC-DT10 rCONP, rCONP was associated with the cell membrane for both of the two cell lines. There is an apparent increase in fluorescent intensity when cells are incubated with higher concentration (12.5 $\mu\text{g/ml}$, Panels C and F in Fig. 4) of FITC-DT10 rCONP compared with lower concentration (1 $\mu\text{g/ml}$, Panels A and D in Fig. 4). These results show non-specific interaction of the NPs with the cell membrane and the passive uptake of FITC-DT10 rCONP. The interaction and internalization of NPs with cells are influenced by surface functionalization, size and shape of the NPs as well as cell type.^{40, 41} The intracellular localization and internalization pathway of FITC-DT10 rCONP needs to be further investigated. This multi-component rCONP platform could be used for multiple applications such as determination of *in vitro* cellular trafficking and for *in vivo* fluorescent imaging by functionalizing NPs with near-infrared dyes. This method will also allow for the determination of cellular localization of rCONP conjugated with targeting molecules which can enhance cellular uptake through receptor mediated endocytosis. These are currently being investigated in our laboratory.

3.5 Biodistribution and SPECT imaging of PAA, DT10 and functionalized DT10 coated rCONP

Biodistribution studies of PAA, DT10 and functionalized DT10 rCONP based on gamma counting indicated obvious differences in biodistribution according to their surface coating and size. The uptake (%ID/g) values of PAA and DT10 ¹⁴¹Ce-rCONP in blood and major organs collected from nude mice at different time points post tail vein injection (5 min, 1 hr, 4 hrs, 24 hrs, 48 hrs, 120 hrs; n=3 per time point) are plotted in Fig. 5. PAA ¹⁴¹Ce-rCONP showed rapid clearance from the blood pool (within 10 min), which could be due to its smaller HD size (~2 nm), whilst DT10 ¹⁴¹Ce-rCONP showed a blood circulation half life of 27 min. The marginally longer blood circulation of DT10 ¹⁴¹Ce-rCONP could be attributed to its relatively bigger HD size (6 nm), which is slightly above the renal filtration threshold of 5.5 nm, determined by others using a different class of NPs.⁴² The

¹⁴¹Ce-rCONP washed out of the heart and lung with the circulation and rapid uptake in liver and spleen was observed 40 after clearing from the blood pool within 1 hr (PAA ¹⁴¹Ce-rCONP) or 4 hrs (DT10 ¹⁴¹Ce-rCONP). For DT10 ¹⁴¹Ce-rCONP, the uptake in the liver reached a maximum at 4 hrs and then gradually reduced over a period of several days, while the uptake in the spleen increased over time. This pattern was also 45 confirmed by *in vivo* SPECT imaging. PAA ¹⁴¹Ce-rCONP showed the highest uptake at 1 hr in the liver and spleen then gradually cleared during the investigated time points. The rapid clearance of PAA ¹⁴¹Ce-rCONP also results in a lower uptake in liver and spleen compared to DT10 ¹⁴¹Ce-rCONP. Overall, 50 different biodistribution profiles and pharmacokinetics of PAA and DT10 ¹⁴¹Ce-rCONP originated from different their sizes and surface coatings. Biodistribution of DT10-PEG and DT10-SB ⁶⁵Zn-rCONP was obviously different from DT10 ¹⁴¹Ce-rCONP, which is shown in Fig. S7. Interestingly, the accumulation of both 55 DT10-PEG and DT10-SB ⁶⁵Zn-rCONP in liver gradually decreased from ~25% ID/g at 1 hr to < 10% ID/g at 48 hrs, which is obvious lower than DT10 ¹⁴¹Ce-rCONP. However, their uptake in heart, lung, intestine and skin was much higher than DT10 ¹⁴¹Ce-rCONP. Higher uptake in kidneys of PAA ¹⁴¹Ce-rCONP 60 was also observed, which could be due to both cellular uptake and renal clearance. All of these observations reflect the significant effect of HD size and surface functionalization on the biodistribution of rCONP.

Smaller HD size of PAA ¹⁴¹Ce-rCONP is beneficial in terms of 65 renal clearance. Rapid clearance of rCONPs reduces nonspecific accumulation, which could decrease tissue toxicity and improve contrast for *in vivo* molecular imaging. To further reduce potential toxicity, rCONP could be synthesized with higher specific activity, thereby decreasing the overall mass of 70 administered radiolabeled nanoprobe. Furthermore, the HD size of DT10-NH₂ ¹⁴¹Ce-rCONP can be further manipulated to yield ultrasmall rCONP of HD size 1~3 nm, similar to PAA ¹⁴¹Ce-rCONP, as shown in Fig. S2F.



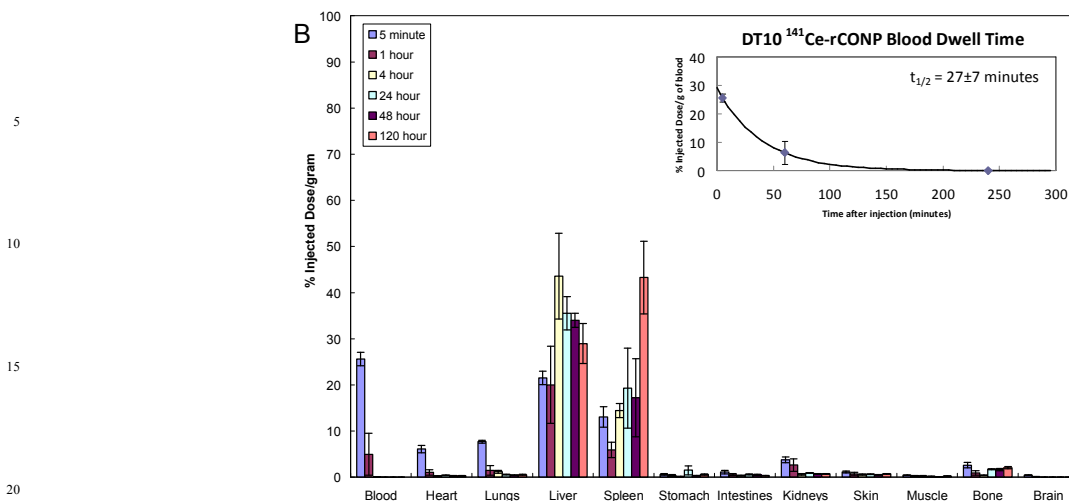


Fig. 5 Biodistribution (%ID/g) at various time points post i.v. administration of (A) PAA ¹⁴¹Ce-rCONP and (B) DT10 ¹⁴¹Ce-rCONP. The figure inserts show the best-fit curve of the respective ¹⁴¹Ce-rCONP (%ID/g) time activity curves in blood. The calculated half-lives ($t_{1/2}$) of PAA ¹⁴¹Ce-rCONP and DT10 ¹⁴¹Ce-rCONP in blood are 8.8 min and 27 min respectively.

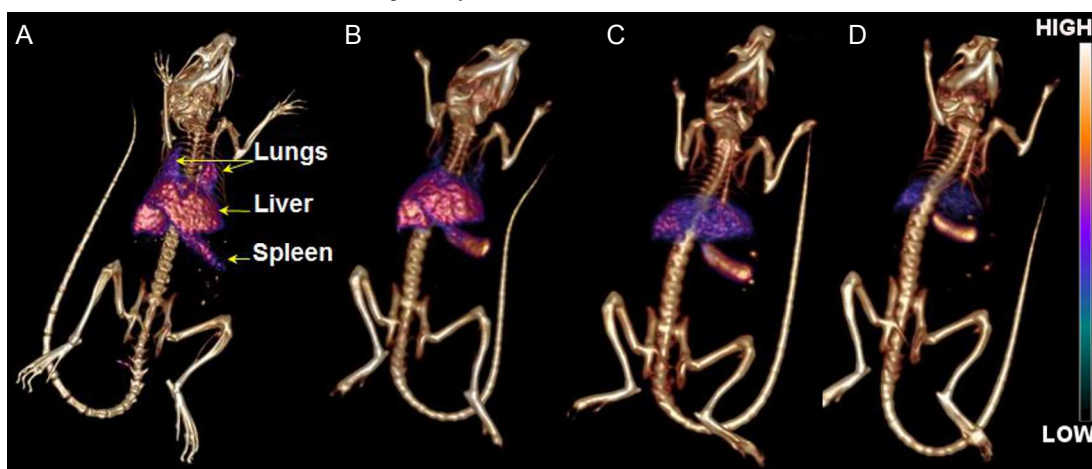


Fig. 6 *In vivo* SPECT/CT imaging of a nude mouse injected with DT10 ¹⁴¹Ce-rCONP (~180 μ Ci, 3.6 nmole, 250 μ L), at (A) 2 hrs, (B) 24 hrs, (C) 72 hrs and (D) 144 hrs post injection. Images shown here were obtained from volume renderings that were adjusted to a uniform scale.

Real time SPECT/CT imaging was demonstrated in a nude mouse injected with DT10 ¹⁴¹Ce-rCONP (182 μ Ci, 335 μ L, 3.6 nmole, specific activity is 50.6 mCi/ μ mol) was acquired following the time points (2 hrs, 24 hrs, 72 hrs and 144 hrs) (Fig. 6 and S8). After 2 hrs of injection, ¹⁴¹Ce-rCONP predominantly accumulated in lungs, liver and spleen and then gradually cleared from the lungs but was still retained in liver and spleen 24 hrs post injection. It is not surprising that ¹⁴¹Ce-rCONP accumulated in reticuloendothelial system (RES) early after injection because macrophages tend to capture and scavenge NPs from the blood circulation through opsonization.⁴³ However, the uptake of ¹⁴¹Ce-rCONP in the spleen was found to gradually increase over a period of days. This might be due to the redistribution of cleared ¹⁴¹Ce-rCONP from the lungs, liver and other tissues, which are then taken up by some specific phagocytes in the spleen. DT10 coated iron oxide nanoparticles have been used by others to label macrophages through nonspecific uptake mechanisms.⁴⁴ Similarly, DT10 ¹⁴¹Ce-rCONP could have been taken up by macrophages. Further investigations are needed to understand the interaction of DT10 ¹⁴¹Ce-rCONP with macrophages and other tissues *in vivo*. Although the quantity of ¹⁴¹Ce-rCONP injected

for SPECT imaging was relatively quite high, the pattern of DT10 ¹⁴¹Ce-rCONP *in vivo* distribution observed through SPECT imaging is largely consistent with the results of *ex vivo* biodistribution study (Fig. 5, 6 and S8). It also reflects the high stability of intrinsically radiolabeled DT10 CONP *in vivo*. It should be pointed out that the radiolabeling strategy provides a robust method to accurately monitor the fate of CONP *in vivo* which is important to further understand the relationship between the surface modification of NPs and their *in vivo* behavior. To the best of our knowledge, this is the first time that real time *in vivo* pharmacokinetics of CONP was monitored by radiotracer techniques. Using the strategy described in this paper, it is also possible to incorporate positron emitting isotopes into CONP for PET imaging. The facile radiolabeling and multifunctionalization strategy, low toxicity and high bio-stability of rCONP make it a promising *in vivo* quantitative tool to understand the mechanisms underlying the radioprotective properties of CONP.

4. Conclusions

In summary, we demonstrated a general strategy to synthesize multifunctional intrinsic rCONP. Neither the chemical nor

physical properties of rCONP were changed by the incorporation of trace radioisotopes. The physiological properties and pharmacokinetics of CONP can be adjusted by modifying their surface coating. The cell viability, cell uptake and biodistribution of rCONP indicated obvious correlation to its surface coating and size. FITC conjugated rCONP can be used for cell labeling. Real time *in vivo* SPECT imaging of DT10 ¹⁴¹Ce-rCONP was acquired and clearly showed the evolution of pharmacokinetics of CONP, reflecting the data obtained by *ex vivo* biodistribution study. Our radiolabeling method makes it feasible to monitor the evolution of CONP *in vivo* and multifunctional rCONP could be potentially utilized as a novel nanomedicine for multiple biomedical imaging and theranostic applications.

Acknowledgments

This work was funded in part by VCU School of Medicine. We would like to thank Dr. Jerry Hirsch, Dr. Gajanan Dewkar, Ms. Celina Thadigiri and Dr Atul Asati (UCF-NSTC) for technical assistance. We acknowledge Dr Everett. E. Carpenter and Dr Joseph Turner (Department of Chemistry, Virginia Commonwealth University) for kind assistance with DLS and ICP measurement. And we also thank to Mary Embree and Maryna Kuchuk (Research Reactor Center, University of Missouri, Columbia, Missouri) for the ¹⁴¹Ce production.

Notes

^aCenter for Molecular Imaging, Department of Radiology, School of Medicine, Virginia Commonwealth University, Richmond, Virginia, USA, 23298. Fax: +1 804 6280223; Tel: +1 804 6282791; Email: jzweit@vcu.edu
^bResearch Reactor Center, University of Missouri, Columbia, Missouri, USA, 65211. Fax: +1 573 8826360; Tel: +1 573 8825211;
^cNanoscience Technology Center, University of Central Florida, Orlando, Florida, USA, 32826. Tel: +1 407 882 2843.
 † Electronic Supplementary Information (ESI) available: [HPLC for DT10 ¹⁴¹Ce-rCONP and DT10-PEG and DT10-SB ⁶⁵Zn-rCONP, DLS of rCONP with all types of coatings, NMR of PEG and SB functionalized DT10, TGA of DT10-NH₂ CONP, redox properties of DT10 ¹⁴¹Ce-rCONP, cell viability of ¹⁴¹Ce-rCONP in A549 and SK-OV-3 cell lines, biodistribution of DT10-PEG and DT10-SB ⁶⁵Zn-rCONP and quantitative analysis of micro-SPECT images of one mouse injected with DT10-¹⁴¹Ce-rCONP]. See DOI: 10.1039/b000000x/

References

- 1 R. K. Jain, *Adv. Drug. Deliv. Rev.*, 2001, **46**, 149.
- 2 J. Cheon, J-H. Lee, *Acc. Chem. Res.*, 2008, **41**, 1630.
- 3 G. V. Maltzahn, J-H. Park, K. Y. Lin, N. Singh, C. Schwöppe, R. Mesters, W. E. Berdel, E. Ruoslahti, M. J. Sailor and S. N. Bhatia, *Nat. Mater.*, 2011, **10**, 545 and references therein.
- 4 M. Ferrari, *Nat. Rev.*, 2005, **5**, 161.
- 5 M. Das, S. Patil, N. Bhargava, J-F. Kang, L. M. Riedel, S. Seal and J. J. Hickman, *Biomaterials*, 2007, **28**, 1918.
- 6 S. M. Hirst, A. S. Karakoti, R. D. Tyler, N. Sriranganathan, S. Seal and C. M. Reilly, *Small*, 2009, **5**, 2848.
- 7 A. Gojova, J. Lee, H. S. Jung, B. Guo, A. I. Barakat and I. M. Kennedy, *Inhal. Toxicol.*, 2009, **21**, 123.
- 8 I. Celardo, M. D. Nicola, C. Mandoli, J. Z. Pedersen E. Traversa and L. Ghibelli, *ACS Nano*, 2011, **5**, 4537.
- 9 S. M. Hirst, A. Karakoti, S. Singh, W. Self, R. Tyler, S. Seal, and C. M. Reilly, *Environ. Toxicol.*, 2011, **1**.
- 10 B. A. Rzigalinski, K. Meeharr, R. M. Davis, Y. Xu, W. C. Miles and C. A. Cohen, *Nanomedicine*, 2006, **1**, 399.
- 11 J. M. Perez, A. Asati, S. Nath and C. Kaittanis, *Small*, 2008, **4**, 552.

- 12 Y. Peng, X. Chen, G. Yi and Z. Gao, *Chem. Commun.*, 2011, **47**, 2916.
- 13 A. Atul, S. Santra, C. Kaittanis, S. Nath and J. M. Perez, *Angew. Chem. Int. Ed.*, 2009, **48**, 2308.
- 14 A. Asati, S. Santra, C. Kaittanis and J. M. Perez, *ACS Nano*, 2010, **4**, 5321.
- 15 L. Kong, X. Cai, X. Zhou, L. L. Wong, A. S. Karakoti, S. Seal and J. F. McGinnis, *Neurobiol. Dis.*, 2011, **42**, 514.
- 16 J. Colon, N. Hsieh, A. Ferguson, P. Kupelian, S. Seal, D. W. Jenkins and C. H. Baker, *Nanomed. Nanotechnol.*, 2010, **6**, 698.
- 17 R. W. Tarnuzzer, J. Colon, S. Patil and S. Seal, *Nano Lett.*, 2005, **5**, 2573.
- 18 D. Schubert, R. Dargusch, J. Raitano and S. Chan, *Biochem. Biophys. Res. Commun.*, 2006, **342**, 86.
- 19 I. Celardo, E. Traversa and L. Ghibelli, *J. Exp. Ther. Oncol.*, 2010, **9**, 47.
- 20 J. Niu, A. Azfer, L. M. Rogers, X. Wang and P. E. Kolattukudy, *Cardiovasc. Res.*, 2007, **73**, 549.
- 21 X. Zhou, L. L. Wong, A. S. Karakoti, S. Seal and J. F. McGinnis, *PLoS One*, 2011, **6**, e16733-1.
- 22 A. sati, C. Kaittanis, S. Santra and J. M. Perez, *Anal. Chem.*, 2011, **83**, 2547.
- 23 K. Susumu, E. Oh, J. B. Delehanty, J. B. Blanco-Canosa, B. J. Johnson, V. Jain, W. J. Hervey, W. R. Algar, K. Boeneman, P. E. Dawson and I. L. Medintz, *J. Am. Chem. Soc.*, 2011, **133**, 9480.
- 24 A. Verma and F. Stellacci, *Small*, 2010, **6**, 12.
- 25 M. Zhou, R. Zhang, M. Huang, W. Lu, S. Song, M. P. Melancon, M. Tian, D. Liang and C. Li, *J. Am. Chem. Soc.*, 2010, **132**, 15351.
- 26 W. Cai, K. Chen, Z. B. Li, S. S. Gambhir and X. Chen, *J. Nucl. Med.*, 2007, **48**, 1862.
- 27 F. Ducongé, T. Pons, C. Pestourie, L. Hérin, B. Thézé, K. Gombert, B. Mahler, F. Hinnen, B. Kühnast, F. Dollé, B. Dubertret and B. Tavitian, *Bioconjugate. Chem.*, 2008, **19**, 1921.
- 28 M. H. Sun, D. Hoffman, G. Sundaresan, L. Yang, N. Lamichhane and J. Zweit, *Am. J. Nucl. Med. Mol. Imaging*, 2012, **2**, 122.
- 29 E. Muro, T. Pons, N. Lequeux, A. Fragola, N. Sanson, Z. Lenkei and B. Dubertret, *J. Am. Chem. Soc.*, 2010, **132**, 4556.
- 30 W. Liu, A. B. Greytak, J. Lee, C. R. Wong, J. Park, L. F. Marshall, W. Jiang, P. N. Curtin, A. Y. Ting, D. G. Nocera, D. Fukumura, R. K. Jain and M. G. Bawendi, *J. Am. Chem. Soc.*, 2010, **132**, 472.
- 31 Y. Ju-Nam and J. R. Lead, *Sci. Tot. Environ.*, 2008, **400**, 396.
- 32 X. He, H. Zhang, Y. Ma, W. Bai, Z. Zhang, K. Lu, Y. Ding, Y. Zhao and Z. Chai, *Nanotechnology*, 2010, **21**, 285103-1.
- 33 F. Simonelli, P. Marmorato, K. Abbas, J. Ponti, J. Kozempel, U. Holzwarth, F. Franchini and F. Rossi, *IEEE Trans. Nanobiosci.*, 2011, **10**, 44.
- 34 F. Zhang, C. Chen, J. M. Raitano, J. C. Hanson, W. A. Caliebe, S. Khalid and S. Chan, *J. Appl. Phys.*, 2006, **99**, 084313-1.
- 35 S. Babu, A. Schulte and S. Seal, *Appl. Phys. Lett.*, 2008, **92**, 123112-1.
- 36 V. Esposito and E. Traversa, *J. Am. Ceram. Soc.*, 2008, **91**, 1037.
- 37 A. S. Karakoti, S. V. N. T. Kuchibhatla, K. S. Babu and S. Seal, *J. Phys. Chem. C*, 2007, **111**, 17232.
- 38 E. Herz, A. Burns, D. Bonner and U. Wiesner, *Macromol. Rapid Commun.*, 2009, **30**, 1907.
- 39 M. J. Murcia and C. A. Naumann, *Nanotechnologies for the Life Sciences*, ed C. S. S. R. Kumar, WILEY-VCH Verlag GmbH & Co. KGaA, Weinheim, 1st edn., 2005, Vol. 1, pp. 3.
- 40 A. E. Nel, L. Madler, D. Velegol, T. Xia, E. M. Hoek, P. Somasundaran, F. Klaessig, V. Castranova and M. Thompson, *Nat. Mater.*, 2009, **8**, 543.
- 41 V. Biju, T. Itoh and M. Ishikawa, *Chem. Soc. Rev.*, 2010, **39**, 3031.
- 42 H. S. Choi, W. Liu, P. Misra, E. Tanaka, J. P. Zimmer, B. I. Ipe, M. G. Bawendi and J. V. Frangioni, *Nat. Biotechnol.*, 2007, **25**, 1165.
- 43 M. L. Schipper, G. Iyer, A. L. Koh, Z. Cheng, Y. Ebenstein, A. Aharoni, S. Keren, L. A. Bentolila, J. Li, J. Rao, X. Chen, U. Banin, A. M. Wu, R. Sinclair, S. Weiss and S. S. Gambhir, *Small*, 2009, **5**, 126.
- 44 M. Nahrendorf, H. W. Zhang, S. Hambrador, P. Panizzi, D. E. Sosnovik, E. Aikawa, P. Libby, F. K. Swirski and R. Weissleder, *Circulation*, 2008, **117**, 379.